JOURNAL OF SOLID STATE CHEMISTRY 137, 161–167 (1998)
ARTICLE NO. SC987748

An *in Situ* Temperature-Dependent Electron and X-ray Diffraction Study of Structural Phase Transitions in ZrV_2O_7

R. L. Withers,*,[1] J. S. O. Evans,† J. Hanson,‡ and A. W. Sleight‡

*Research School of Chemistry, Australian National University, Canberra, A.C.T, 0200 Australia; †Department of Chemistry, Brookhaven National Laboratory, Upton, New York; and ‡Department of Chemistry, Oregon State University, Corvallis, Oregon 97331

A detailed electron diffraction study has been made of the ZrV_2O_7 member of the AM_2O_7 family of displacively flexible framework structures and its temperature-dependent structural phase transformations. The phase below 77°C corresponds to a primitive 3×3×3 superstructure phase of $Pa\bar{3}$ space group symmetry while the high temperature phase above 102°C corresponds to the normal parent structure. The intervening intermediate phase is a complex incommensurately modulated phase characterized by (more than one) incommensurate primary modulation wave-vector in the close vicinity of $\frac{1}{3}\langle 110\rangle^*$. The cubic point group symmetry of this intervening incommensurate phase is shown to be lowered from cubic *m*3*m*. No corresponding metrical strain distortion can be detected.

1. INTRODUCTION

A large family of cubic AM_2O_7 compounds is known whose ideal (usually high temperature) framework structure has space group symmetry $Pa\bar{3}$, $Z = 4$ and is built out of corner-connected AO_6 octahedra and MO_4 tetrahedra, as shown in Fig. 1 (1–3). There has been long-standing interest in this AM_2O_7 family of compounds because of their low isotropic thermal expansion above a normal to $3 \times 3 \times 3$ superstructure phase transition, which usually occurs above room temperature in the range 100–400°C (1–5). Displacively flexible, corner-connected framework structures of this type (e.g., the low pressure polymorphs of silica, perovskite, etc.) often exhibit unusual thermal expansion properties and are susceptible to displacive structural phase transformation involving rotation of essentially rigid framework polyhedra (6–8). In the case of SiO_2 quartz, for example, the existence of an apparently simple displacive structural phase transformation at ~ 573°C involving coupled rotation of corner-connected SiO_4 tetrahedra has long been known. (Interestingly, *in situ* TEM studies of this phase transformation subsequently showed that the phase transition was not so simple and revealed the existence of an intervening intermediate incommensurate phase separating the low temperature α-form from the high temperature β-form.)

Recently there has been particular interest in the ZrV_2O_7 member of the AM_2O_7 family of compounds because of its strong and isotropic negative thermal expansion above about 100°C all the way up to about 800°C (1–3). DSC measurements on ZrV_2O_7 showed that the onset of negative thermal expansion in this material occurs at the same temperature as a well defined structural phase transition at 102°C. They also, however, revealed the existence of a further sharp phase transition at 77°C (1–3). Thermal expansion measurements (see Fig. 2) likewise show the existence of two separate phase transitions. Neutron and X-ray diffraction data were reported to show a $3 \times 3 \times 3$ superstructure below and above the 77°C transition but not above the 102°C transition (1). The nature of the intermediate phase between the room temperature $3 \times 3 \times 3$ superstructure phase and the high temperature ideal structure thus remains unclear. The purpose of this paper is to present the results of an *in situ* electron difraction (ED) study of this intermediate phase and the temperature-dependent structural phase transitions of ZrV_2O_7.

2. EXPERIMENTAL

The synthesis of the ZrV_2O_7 used in this study is described in Refs. (1, 3). Specimens for electron microscopy were prepared by crushing and dispersing onto holey-carbon coated molybdenum grids. These grids were then examined in JEOL 100CX and Philips EM430 transmission electron microscopes (TEMs). The temperature-dependent TEM work was carried out in the JEOL 100CX TEM using an EM-SHTH2 double tilt heating holder. Specimen tilt was extremely limited ($\sim \pm 3°$) about the second tilt axis, severely limiting the ability to systematically investigate reciprocal space. Likewise, knowledge of the absolute temperature at any particular grain was not possible as the local temperature depends, among other factors, on the proximity of the

[1] To whom correspondence should be addressed.

0022-4596/98 $25.00

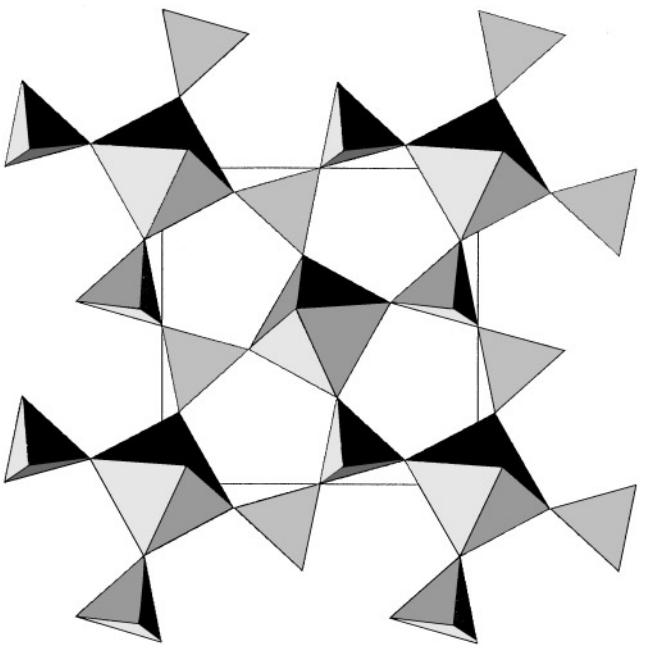

FIG. 1. Shows the ideal AM_2O_7 framework structure projected along an $\langle 001 \rangle$ direction. The unit cell is outlined. The structure is built out of corner-connected AO_6 octahedra and MO_4 tetrahedra. There exist two such layers per unit cell. For the purposes of clarity, only one of these layers is shown. The other is related via an *a* glide.

particular grain being investigated to the molybdenum grid bars. The XRD data was collected on beam line X7b at the National Synchrotron Light Source (NSLS), Brookhaven using a Fuji image plate system with offline scanners. Temperature control was via an Oxford instruments cryostream. Denzo software was used to obtain integrated intensities.

3. RESULTS

As expected, the ED results show that the phase below 77°C (~350 K) corresponds to a primitive $3 \times 3 \times 3$ superstructure phase (see Figs. 3a–5a). The characteristic extinction condition ($F(hk0) = 0$ unless h is even) apparent in electron diffraction patterns (EDPs) at $\langle 001 \rangle$ zone axis orientations of this phase (see Fig. 3a; note that reflections indexed as [200]* and [010]* in Fig. 3b become [600]* and [030]* in Fig. 3a when indexed with respect to the $3 \times 3 \times 3$ superstructure) necessitates the existence of an *a* glide and definitively confirms the *Pa* portion of the $Pa\bar{3}$ space group symmetry reported for this phase (the possibility was recently raised (3) that the room temperature space group symmetry might be of lower symmetry than $Pa\bar{3}$, e.g., $P2_13$, $R\bar{3}$, or $R3$).

Likewise, the absence of satellite reflections above the second phase transition at ~100°C is consistent with a high-temperature normal, or unmodulated, phase. (Despite evidence for large amplitude transverse thermal motion of oxygen atoms in this phase (3), there is no obvious corresponding diffuse intensity distribution apparent in EDPs.) The strong Bragg reflections corresponding to this underlying parent structure, and in common for all three phases, are hereafter labelled **G** in what follows. Indexation of the $\langle 001 \rangle$, $\langle \bar{1}2\bar{2} \rangle$, and $\langle 102 \rangle$ zone axis EDPs of Figs. 3–5 is always with respect to this underlying parent structure. (Note that the use of angled brackets for the intermediate incommensurate phase is not strictly justified as the local point group symmetry of the intermediate phase is not known (see below). The angled brackets in this case should be thought of as referring only to the underlying parent structure.)

The intermediate phase between 77 and 102°C is characterized by incommensurate satellite reflections, by far the strongest of which fall in the close vicinity of $\mathbf{G} \pm \frac{1}{3}\langle 110 \rangle^*$ regions of reciprocal space (see Figs. 3–5). From a modulation wave point of view, the primary modulation wavevectors (9) characteristic of this intermediate incommensurate phase are thus of $\mathbf{q} \sim \frac{1}{3}\langle 110 \rangle^*$ type. The question of how many distinct such $\sim \frac{1}{3}\langle 110 \rangle^*$ modulations locally coexist, however, is extremely difficult to answer. Given cubic parent symmetry, there are six such $\sim \frac{1}{3}\langle 110 \rangle^*$ modulations possible. Resultant cubic symmetry for this intermediate incommensurate phase would thus require at least six such modulations to coexist simultaneously.

That not all six such modulations locally co-exist is apparent from $\langle \bar{1}2\bar{2} \rangle$ zone axis EDPs, such as Fig. 4b, for example, where $\mathbf{G} \pm \sim \frac{1}{3}[101]^*$ type satellite reflections are clearly present (note that modulation wave-vectors are only defined to within an allowed parent Bragg reflection so that $\mathbf{G} \pm \frac{1}{3}[\bar{2}01]^* \equiv \mathbf{G}' \pm \frac{1}{3}[101]^*$ etc.) but where $\mathbf{G} \pm \sim \frac{1}{3}[\bar{1}10]^*$ ($\mathbf{G} \pm \frac{1}{3}[210]^* \equiv \mathbf{G}' \pm \frac{1}{3}[\bar{1}10]^*$) and $\mathbf{G} \pm \sim \frac{1}{3}[011]^*$ type satellite reflections are equally clearly not present. This result requires that the cubic *m*3*m* point group symmetry of the reciprocal lattice of the parent structure is definitely lowered for the intermediate incommensurate phase, although to exactly what remains to be determined. Despite the clear lowering in point group symmetry, there is no corresponding resultant strain distortion detectable (1–3). Such a situation, while rare, is not unknown—particularly for modulated structures of this type (10–13).

Accurate measurement of the position of incommensurate satellite reflections via ED is inherently rather less accurate than via XRPD. As well as can be measured, however, the incommensurate satellite reflections in Fig. 4b fall at the $\mathbf{G} \pm 0.312(3)$ $[\bar{2}01]^* \equiv \mathbf{G}' \pm [0.376, 0, 0.312]^*$ positions of reciprocal space. It should be borne in mind, however, that there is some evidence that the positions of the incommensurate satellite reflections are temperature-dependent within the temperature range of existence of this incommensurate phase. Unfortunately, because of the experimental conditions obtaining, it is not possible to know exact local temperatures.

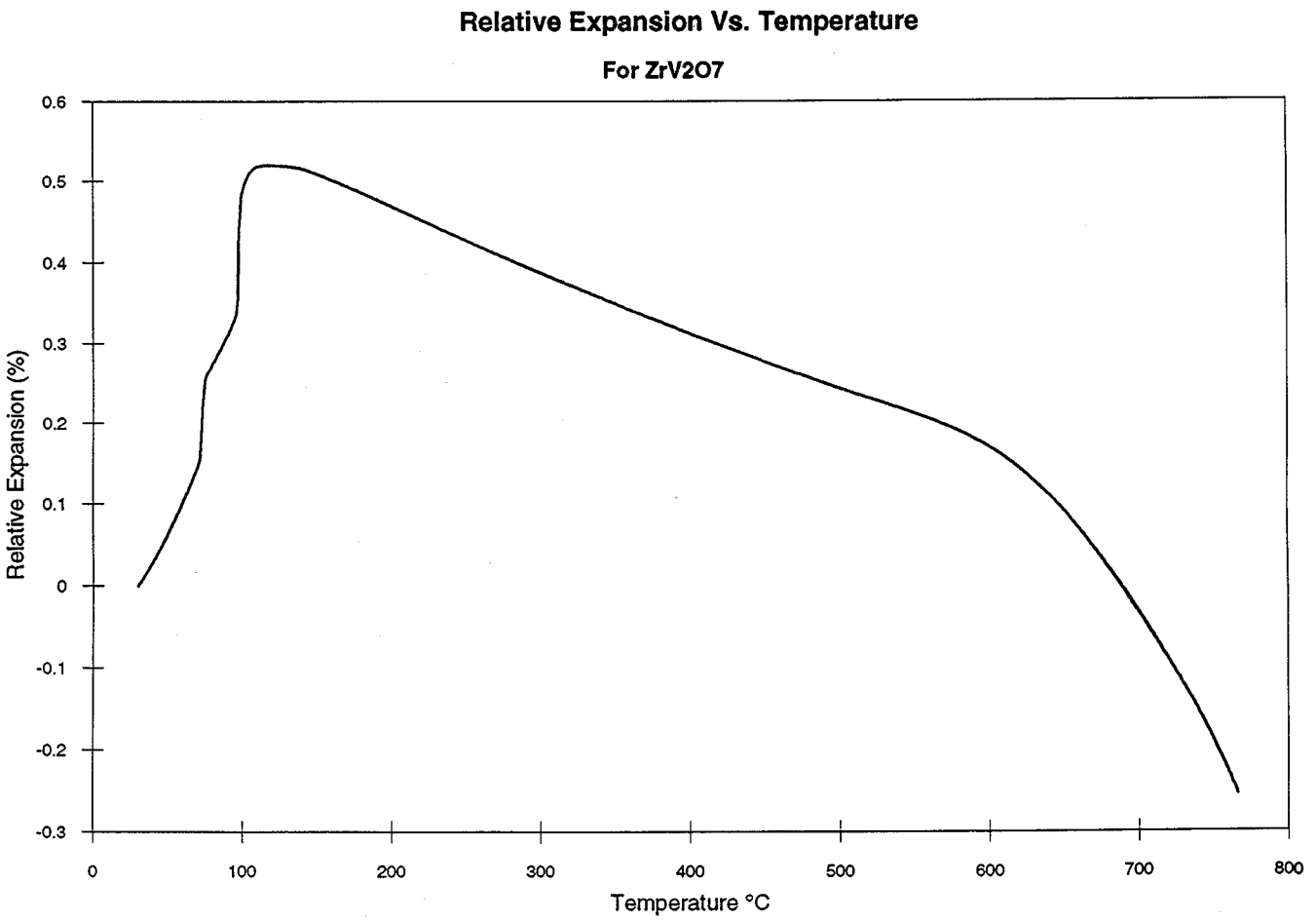

FIG. 2. Plot of the relative expansion of the underlying cubic unit cell parameter of ZrV_2O_7 as a function of temperature. Note the two phase transitions apparent at 77 and 102°C.

While Fig. 4b shows that it is possible to find large enough single domain areas to demonstrate that not all six possible $\sim\frac{1}{3}\langle 110\rangle^*$ modulations locally coexist, it is more normally the case that all the six possible $\mathbf{G} \pm \sim\frac{1}{3}\langle 110\rangle^*$ type satellite reflections appear in both selected area, as well as focused probe ($\sim$500–1000 Å) micro-diffraction, EDPs (if not in the zero order Laue zone, or ZOLZ, then in the higher order Laue zone, or HOLZ, rings—cf., for example, the superlattice HOLZ rings in Fig. 5b) of this intermediate incommensurate phase, thereby implying relatively fine scale twinning. Given the existence of a cubic parent structure in conjunction with the apparent absence of metrical strain distortion, such fine scale twinning is only to be expected and makes it extremely difficult to be sure how many such modulations coexist in any one local area. Similar multi-**q** problems are well known in the field of, for example, charge density wave modulated structures and other such systems (10–14).

Apart from the incommensurability of the primary modulation wave-vectors, the major distinction between this intermediate incommensurate phase and the low temperature "locked-in" $3 \times 3 \times 3$ superstructure phase is the virtually complete absence of higher order harmonic satellite reflections (such as those of $\mathbf{G} \pm \frac{1}{3}\langle 001\rangle^*$ or $\mathbf{G} \pm \frac{1}{3}\langle 111\rangle^*$ type) in the intermediate phase compared to the room temperature phase (cf., for example, the $\langle 001\rangle$ (Fig. 3), $\langle \bar{1}2\bar{2}\rangle$ (Fig. 4), and $\langle 102\rangle$ (Fig. 5) zone axis EDPs characteristic of the two phases).

This is also clearly apparent in the reflection statistics of the "single crystal" XRD data (see Table 1). The number of reflections $> 9\sigma$ with no index = 3n (i.e., reflections of $\mathbf{G} \pm \sim\frac{1}{3}\langle 111\rangle^*$ type) drops several orders of magnitude (from 1141 to 4) on heating from room temperature to 90°C. Similarly, the number of reflections $> 9\sigma$ with two indices = 3n (i.e., reflections of $\mathbf{G} \pm \sim\frac{1}{3}\langle 001\rangle^*$ type) also drops several orders of magnitude (from 950 to 8) on heating from room temperature to 90°C, whereas the number of reflections $> 9\sigma$ with only one index = 3n (i.e., the first order harmonic satellite reflections of the $\mathbf{G} \pm \sim\frac{1}{3}\langle 110\rangle^*$ type) only drops by a factor of $\sim$3 (from 2,608 to 871). Note that

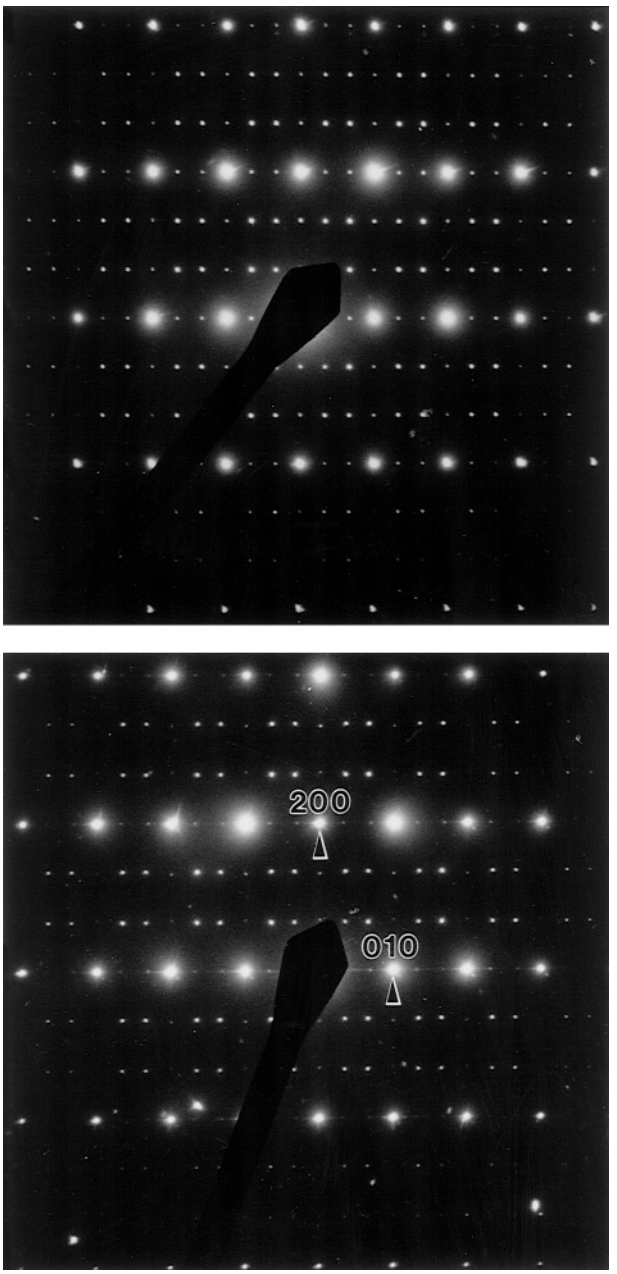

FIG. 3. $\langle 001 \rangle$ zone axis EDPs typical of (a) the room temperature $3 \times 3 \times 3$ superstructure phase and (b) the intermediate incommensurate phase. Indexation in (b) is with respect to the underlying parent structure.

h, k, l in Table 1 corresponds to indexation with respect to the low temperature $3 \times 3 \times 3$ superstructure phase.

Careful monitoring of the integrated intensities of the various classes of reflections as a function of temperature shows that the parent reflections tend to diminish least in intensity as a function of increasing temperature while the primary or first order satellite reflections (of $\mathbf{G} \pm \sim\frac{1}{3}\langle 110 \rangle^*$ type) tend to decrease in intensity more or less linearly up to and through the low temperature $3 \times 3 \times 3$-to-incommensurate phase transition (see Fig. 6). By contrast, the integrated intensities of the higher order harmonic satellite reflections (of $\mathbf{G} \pm \frac{1}{3}\langle 001 \rangle^*$ or $\mathbf{G} \pm \frac{1}{3}\langle 111 \rangle^*$ type) tend to fall off discontinuously to virtually zero at this low temperature $3 \times 3 \times 3$-to-incommensurate phase transition (see Fig. 6).

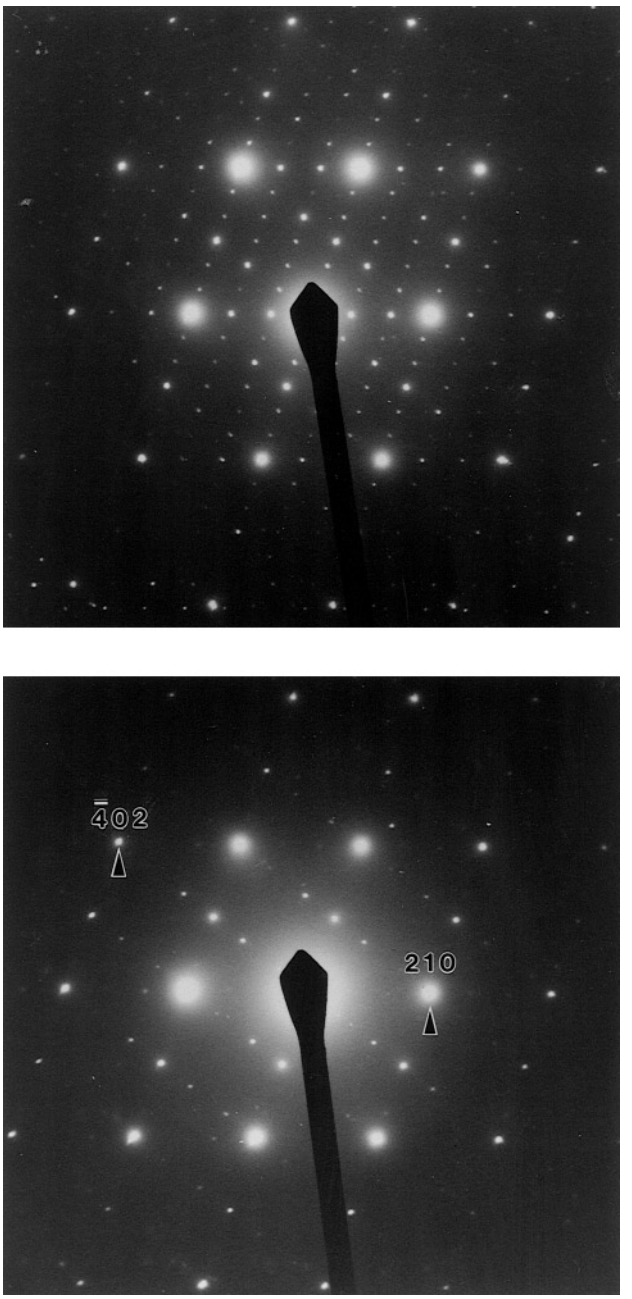

FIG. 4. $\langle \bar{1}2\bar{2} \rangle$ zone axis EDPs typical of (a) the room temperature $3 \times 3 \times 3$ superstructure phase and (b) the intermediate incommensurate phase. The EDP in (b) was obtained from exactly the same grain as was used to obtain (a). Note the disappearance of satellite reflections along the [210]* and [022]* directions of reciprocal space in (b).

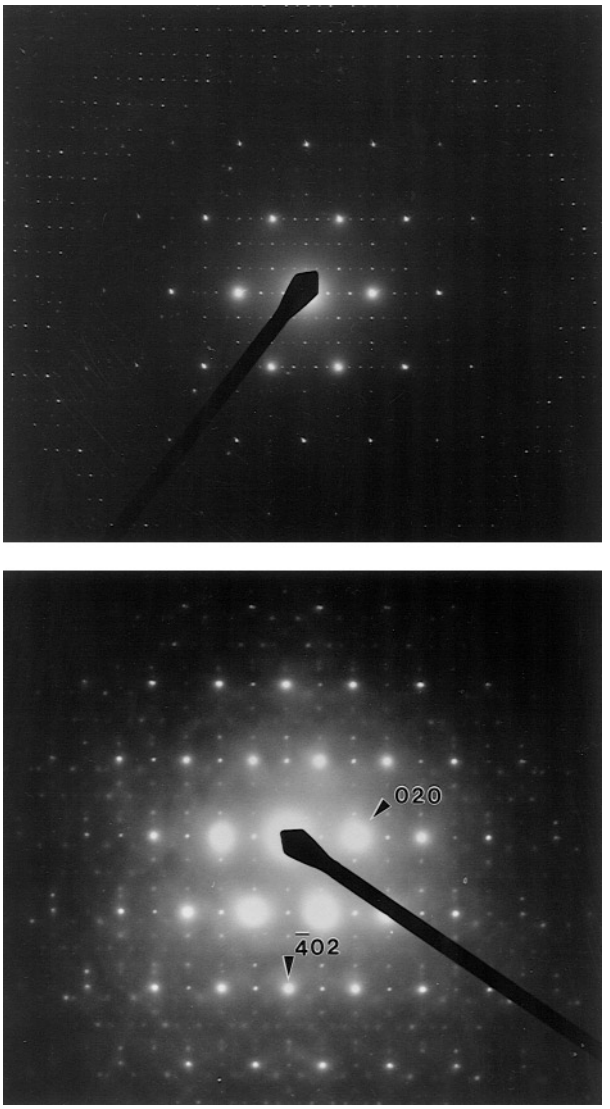

FIG. 5. $\langle 102 \rangle$ zone axis EDPs typical of (a) the room temperature $3 \times 3 \times 3$ superstructure phase and (b) the intermediate incommensurate phase.

In the case of $\langle 001 \rangle$ zone axis EDPs (see Fig. 3b), where typically two distinct $\mathbf{G} \pm \varepsilon\langle 110 \rangle^*$ ($\varepsilon \sim \frac{1}{3}$) type satellite reflections occur in the ZOLZ, higher order harmonic satellite reflections are in fact very weakly visible. (It is in fact the very weak presence of these reflections that makes the incommensurability of the primary modulation wave-vectors immediately apparent in Fig. 3b. Note that the very weak presence of such higher order harmonic satellite reflections in EDPs need not necessarily imply the existence of corresponding displacive modulation waves, i.e., these weak reflections may well be a result of multiple scattering involving the much stronger first order harmonic, or primary, satellite reflections.) In the case of Fig. 3b, the parameter $\varepsilon = 0.345(3)$. Similar EDPs have been obtained, however, with $\varepsilon = 0.352(3)$. It is interesting to note that the deviation of the primary modulation wave-vectors from the ideal $\frac{1}{3}\langle 110 \rangle^*$ position is apparently along the $\langle 110 \rangle^*$ direction of reciprocal space in Fig. 3b but clearly along the $\langle \bar{2}01 \rangle^*$ direction of reciprocal space in Fig. 4b. Presumably this observation rules out the possibility of a single-**q**, incommensurately modulated structure.

While there are distinct differences between the reciprocal lattices of the two phases, close inspection of Figs. 3–5 shows that the two phases also have much in common. The strong incommensurate satellite reflections surrounding the $[\bar{2}01]^*$ parent reflection at $[\bar{2}01]^* \pm 0.314(3)\ [\bar{2}01]^*$ in Fig. 4, for example, are also strong satellite reflections in the corresponding zone axis EDP of the room temperature phase. Similarly, in Figs. 3 and 5 the intensity distribution of the incommensurate $\mathbf{G} \pm \sim\frac{1}{3}\langle 110 \rangle^*$ satellite reflections in closely related to the intensity distribution exhibited by the commensurate $\mathbf{G} \pm \frac{1}{3}\langle 110 \rangle^*$ satellite reflections of the room temperature phase, indicating that the displacive modulation of the framework responsible for these satellite reflections is very similar for the two phases. (Fourier decomposition of an accurate $3 \times 3 \times 3$ superstructure refinement of the low temperature phase should thus give a very good approximation of the atomic modulation function or AMF (9) associated with this incommensurate phase.)

Likewise, the *a* glide extinction characteristic of the room temperature phase when expressed in the language of a modulated structure (namely $F([hk0] \pm \frac{1}{3}\langle 110 \rangle^*) = 0$ unless h is odd) is mirrored in the fact that exactly the same extinction condition is characteristic of the intermediate incommensurate phase (cf., Figs. 3a and 3b), except that now the modulation wave-vector measures 0.345(3) $\langle 110 \rangle^*$ rather than $\frac{1}{3}\langle 110 \rangle^*$ exactly. In the language of superspace groups (and ignoring for the moment the probability that more than one incommensurate $\sim\frac{1}{3}\langle 110 \rangle^*$ modulation might locally coexist in the intermediate phase) the above

TABLE 1
Observed Reflection Statistics at Room Temperature and 90°C

	Room temp.	90°C
Total No. Reflns. measured	10,158	9,482
Total No. Reflns. measured > 0	9,599	7,735
Total No. Reflns. $> 3\sigma$	6,980	2,817
With none of $h, k, l = 3n$	1,859	133
With one of $h, k, l = 3n$	3,384	2,255
With two of $h, k, l = 3n$	1,410	158
With all $h, k, l = 3n$	327	271
Total No. Reflns. $> 9\sigma$	4,990	1,113
With none of $h, k, l = 3n$	1,141	4
With one of $h, k, l = 3n$	2,608	871
With two of $h, k, l = 3n$	950	8
With all $h, k, l = 3n$	291	230

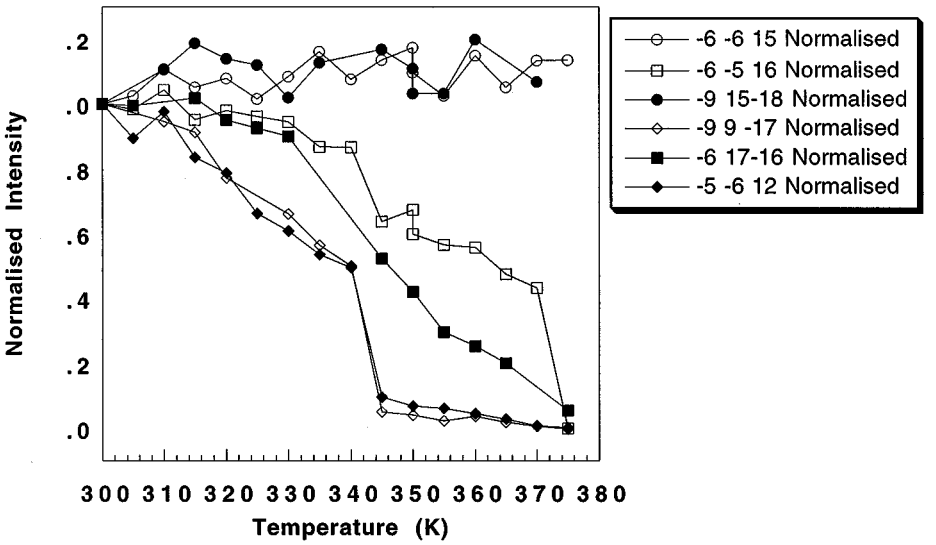

FIG. 6. Shows the integrated intensities of six representative low temperature superstructure reflections as a function of increasing temperature. The $3 \times 3 \times 3$-to-incommensurate phase transition occurs at ~ 343 K. The data for each reflection are normalized to I(300 K) = 1.0.

extinction condition, i.e., $F(hk0m) = 0$ unless $h + m$ is even, implies the existence of a superspace group symmetry operation of the form $\{x_1 + \frac{1}{2}, x_2, -x_3, x_4 + \frac{1}{2}\}$ where $\mathbf{q} \sim \frac{1}{3}\langle 110\rangle^*$ is the incommensurate primary modulation wavevector and constraints the form of the associated AMF (9).

4. DISCUSSION

Low thermal expansion in cubic AM_2O_7 compounds is known to arise as a result of large amplitude transverse thermal motion of the oxygen atoms linking the octahedral and tetrahedral component polyhedral units (1–3, 15–17) of the ideal structure. The tendency of these component polyhedral units to rotate as more or less rigid units implies strongly correlated oxygen atom motion. In the case of ZrV_2O_7, it appears that it is not possible to rotate polyhedra without a small corresponding change in shape of the component polyhedral units (3, 15–17). The rigidity of the component polyhedra is thus an important factor determining the overall flexibility of the framework. Competition between the desire to decrease systematically M–O–M bond angles (requiring polyhedral rotation) and the desire to avoid unreasonable oxygen–oxygen contact distances within the (necessarily somewhat distorted) individual polyhedra suggests some sort of inherent frustration and may be the fundamental reason underlying the existence of an intermediate incommensurate phase separating the high-temperature, supposed normal phase from the low-temperature, $3 \times 3 \times 3$ superstructure phase.

This crystal chemical balance between the desire for tetrahedral rotation and the need to minimize polyhedral distortion can be expected to depend sensitively on the relative size of the cations occupying the component polyhedral units (3) and might be expected to alter the nature of the intervening incommensurately modulated phase. To date, ZrV_2O_7 is the only AM_2O_7 phase known to have an intermediate incommensurate phase. Preliminary ED work, however, shows that ZrP_2O_7 also has an intermediate incommensurate phase (which is *not* isomorphous to that in ZrV_2O_7) despite there being no evidence in either thermal expansion or DSC data for such an intermediate phase (1–3). The ability to predict the existence or otherwise of such an intermediate phase and the nature of the incommensurate phase itself would appear to be a rather good test of our understanding of the detailed crystal chemistry of this intriguing family of materials.

ACKNOWLEDGMENTS

Research was carried out in part at the National Synchrotron Light Source, Brookhaven National Laboratory, which is supported by the US Dept. of Energy, Division of Materials Sciences and Division of Chemical Sciences.

REFERENCES

1. V. Korthuis, N. Khosrovani, A. W. Sleight, N. Roberts, R. Dupree, and W. W. Warren, *Chem. Mater.* **7,** 412 (1995).
2. N. Khosrovani, V. Korthuis, A. W. Sleight, and T. Vogt, *Inorg. Chem.* **35,** 485 (1996).
3. N. Khosrovani, A. W. Sleight, and T. Vogt, *J. Solid State Chem.*, in press.

4. D. F. Craig and F. A. Hummell, *J. Am. Ceram. Soc.* **55,** 532 (1972).
5. R. C. Buchanan and G. W. Wolter, *J. Electrochem. Soc.* **130,** 1905 (1983).
6. A. M. Glazer, *Acta Crystallogr. Sect. B* **28,** 3384 (1972).
7. K. D. Hammonds, M. T. Dove, A. P. Giddy, V. Heine, and B. Winkler, *Am. Mineral.* **81,** 1057 (1996).
8. R. L. Withers and J. G. Thompson, *in* "*In situ* Microscopy in Materials Research." Kluwer, Norwell, MA, 1997.
9. J. M. Pérez-Mato, G. Madariaga, F. J. Zuñiga, and S. A. Garcia Arribas, *Acta Crystallogr. Sect. A* **43,** 216 (1987).
10. R. Vincent and R. L. Withers, *Phil. Mag. Lett.* **56,** 57 (1987).
11. A-K. Larsson, L. Stenberg, and S. Lidin, *Z. Kristallogr.* **210,** 832 (1995).
12. A-K. Larsson, L. Stenberg, and S. Lidin, *Acta Crystallogr. Sect. B* **50,** 636 (1994).
13. D. J. Eaglesham, R. L. Withers, and D. M. Bird, *J. Phys. C* **19,** 359 (1986).
14. R. L. Withers, J. G. Thompson, N. Gabbitas, L. R. Wallenberg, and T. R. Welberry, *J. Solid State Chem.* **120,** 290 (1995).
15. T. A. Mary, J. S. O. Evans, A. W. Sleight, and T. Vogt, *Science* **272,** 90 (1996).
16. J. S. O. Evans, T. A. Mary, T. Vogt, M. A. Subramanian, and A. W. Sleight, *Chem. Mater.* **8,** 2809 (1996).
17. A. K. A. Pryde, K. D. Hammonds, M. T. Dove, V. Heine, J. D. Gale, and M. C. Warren, *J. Phys.: Condens. Matter* **8,** 1 (1996).